Bias-free photoelectrochemical water splitting with photosystem II on a dye-sensitised photoanode wired to hydrogenase

Katarzyna P. Sokol[1], William E. Robinson[1], Julien Warnan[1], Nikolay Kornienko[1],

Marc M. Nowaczyk[2], Adrian Ruff[3], Jenny Z. Zhang[1] and Erwin Reisner[1,*]

(1) Department of Chemistry, University of Cambridge, Lensfield Road, Cambridge CB2 1EW, UK

(2) Plant Biochemistry, Faculty of Biology & Biotechnology, Ruhr-Universität Bochum, Universitätsstr. 150, 44780 Bochum, Germany

(3) Analytical Chemistry - Center for Electrochemical Sciences (CES), Faculty of Chemistry and Biochemistry, Ruhr-Universität Bochum, Universitätsstr. 150, 44780 Bochum, Germany

*Corresponding author: reisner@ch.cam.ac.uk

1

Abstract

Natural photosynthesis stores sunlight in chemical energy carriers, but it has not evolved for the efficient synthesis of fuels, such as H_2. Semi-artificial photosynthesis combines the strengths of natural photosynthesis with synthetic chemistry and materials science to develop model systems that overcome Nature's limitations, such as low-yielding metabolic pathways and non-complementary light absorption by Photosystem (**PS**) **I** and **II**. Here, we report a bias-free semi-artificial tandem platform that wires **PSII** to hydrogenase for overall water splitting. This photoelectrochemical cell integrated the red and blue light-absorber **PSII** with a green light-absorbing diketopyrrolopyrrole dye-sensitised TiO_2 photoanode enabling complementary panchromatic solar light absorption. Effective electronic communication at the enzyme-material interface was engineered using an Os complex-modified redox polymer on a hierarchically-structured TiO_2. This system provides a design protocol for bias-free semi-artificial Z-schemes *in vitro* and provides an extended toolbox of biotic and abiotic components to re-engineer photosynthetic pathways.

Semi-artificial photosynthesis bridges the rapidly progressing fields of synthetic biology and artificial photosynthesis, offering a platform for developing and understanding solar fuel generation[1–4]. Synthetic biology has vastly opened up the way Nature can be manipulated to streamline functionality and to build artificial biological systems, but its complex machineries and metabolic pathways limit engineering flexibility[5]. Artificial photosynthesis utilises synthetic, often biomimetic, components to convert and store solar energy, but is often constrained by inefficient catalysis and costly/toxic materials[6]. Semi-artificial photosynthesis aims to integrate the high efficiency and selectivity of enzymes with the controllability of synthetic materials to photocatalyse endergonic reactions in the absence of competing processes[7]. It also allows the construction of biologically inaccessible pathways with a high level of control and flexibility[3]. The catalytic activity of redox enzymes can be harnessed when adsorbed on electrodes by protein film electrochemistry (PFE) and photoelectrochemistry (PF-PEC)[8,9]. A key challenge is to design biotic-abiotic interfaces that effectively wire together the biological and synthetic components to operate at their optimum.

Solar-driven water splitting into H_2 and O_2 is the most prominent model reaction in artificial photosynthesis[10]. Inefficient catalysis (particularly, kinetically slow O_2 evolution and formation of partially oxidised side products) is a major limitation in synthetic systems, resulting in the requirement of large overpotentials and energy conversion losses[6]. Oxygenic organisms convert solar energy using a photosynthetic Z-scheme containing two light absorbers, Photosystem (**PS**) **I** and **II**[11]. In this tandem configuration, the first excitation in **PSII** drives water oxidation to O_2 and produces a proton gradient, whereas the second excitation in **PSI** generates a low potential electron to drive CO_2 fixation into sugars[12]. Alternatively, H_2 can be produced from microalgae and cyanobacteria, via electron transfer from ferredoxin to a [FeFe]-

hydrogenase (**[FeFe]-H₂ase**), reducing protons to H_2[13]. Efficiencies for photobiological H_2 production are low for several reasons[14,15]. First, **PSII** and **PSI** overlap in light absorption and compete for a small fraction of the solar spectrum. Second, high light intensities limit efficient electron flux up and down-stream of **PSII**. Third, *in vivo* H_2 production relies on O_2-sensitive **[FeFe]-H₂ases**, preventing sustained water splitting. Fourth, CO_2 fixation is preferred over proton reduction leading to low H_2 yields. Overcoming these limitations offers scope for enhancing H_2 production with biological components.

We have previously reported a PEC water splitting system with a **PSII** photoanode wired to a **[NiFeSe]-H₂ase** cathode[3]. However, this system relied solely on light absorption by **PSII** and required an externally applied voltage due to the low electrochemical potential of electrons leaving **PSII**. This limitation can be resolved by introducing a second light absorber to further promote the energetics of the electrons to be delivered to **H₂ase**[16]. To generate sufficient driving force for overall water splitting while maximising solar energy harvesting, complementary dual-absorber/tandem systems can be assembled, showing theoretical limits for solar-to-hydrogen (STH) efficiency of up to 25%[17]. **PSII**[18,19] and $BiVO_4$[20] photoanodes wired to **PSI** photocathodes have been reported to produce electricity, but no chemical fuel. Tandem systems containing **PSII** have not been combined with enzymatic fuel synthesis[21–23].

Herein, a semi-artificial system for unassisted photocatalytic water splitting with **PSII** and **H₂ase** is presented. This PEC system does not require an external energy input as dual light absorption is realised by a tandem photoanode consisting of **PSII** wired to a dye-sensitised TiO_2, providing sufficient voltage to reduce protons using a **H₂ase** cathode. This PEC design is inspired by dye-sensitised solar cells[24,25], and allows

replacing **PSI** by a rationally-designed diketopyrrolopyrrole (**dpp**) dye with an absorption complementary to **PSII**. Efficient electronic communication between **PSII** and **dpp** was achieved by using the redox polymer poly(1-vinylimidazole-*co*-allylamine)-Os(bipy)$_2$Cl (**P$_{Os}$**), which bypasses possible limitations from inefficient interfacial electron transfer. Simultaneously, the hydrogel character of the redox polymer provides a solvated environment for the biocatalyst. A hierarchically-structured inverse opal TiO$_2$ (IO-TiO$_2$) scaffold was employed to provide high surface area for effective integration of polymer/**PSII**.

Assembly of the tandem PSII-dye photoanode

The components and assembly of the PEC tandem cell is depicted in **Fig. 1** and the principle of operation as a semi-artificial Z-scheme is shown in **Supplementary Fig. 1**. Hierarchically-structured IO-TiO$_2$ electrodes were assembled on a TiO$_2$ layer-protected fluorine tin oxide (FTO)-coated glass substrate via a modified co-assembly method (**Supplementary Fig. 2**)[3]. The TiO$_2$ protection layer was used to prevent direct contact of electroactive components (**PSII** and **P$_{Os}$**) with the FTO. The optimal thickness of the IO-TiO$_2$ film was determined to be 20 μm, based on preliminary electrochemical screening, and was utilised throughout this work[4]. Scanning electron microscopy (SEM) revealed a diameter of 750 nm for the TiO$_2$ macropores with connecting channels of 150 nm and a mesoporous skeleton with a porosity of approximately 50 nm. The macroporosity permits the penetration of the bulky **PSII** and **P$_{Os}$** (~20 nm and 16 nm in size, respectively)[3,4], whereas the mesoporous structure provides enhanced effective surface area for guest adsorption.

Dye-sensitisation of the IO-TiO$_2$ photoanodes (A = 0.25 cm^2) was performed by soaking IO-TiO$_2$ in a tetrahydrofuran (THF) solution of **dpp**[26,27] overnight (**Supplementary Fig. 3**). The resulting IO-TiO$_2$|**dpp** electrodes had a **dpp** surface loading of 72 ± 4 nmol cm^{-2} (estimated by spectrophotometry; **Supplementary Fig. 4**), consistent with previously reported loadings of molecular species on mesoporous metal oxide scaffolds[28]. The organic **dpp** dye was selected for its complementary absorption spectrum to **PSII** and for its ability to act as an efficient visible-light photosensitiser for TiO$_2$ in aqueous media, chemisorbing via its phosphonic acid anchoring group[27]. For comparison, electrodes were also prepared using the ruthenium bis(2,2'-bipy)(4,4'-bis(phosphonic acid)-2,2'-bipy) dibromide dye (**RuP;** bipy

= 2,2'-bipyridine)[29–32], which is commonly used as a benchmark in aqueous dye-sensitised schemes (**Supplementary Figs. 1c** and **3**).

The macroporous voids of the IO-TiO$_2$|**dpp** electrodes were subsequently filled with a blend of **PSII** and **P$_{Os}$** to give the fully-integrated IO-TiO$_2$|**dpp**|**P$_{Os}$**−**PSII** tandem photoanode. **PSII** chosen for this study was isolated from the thermophilic cyanobacterium *Thermosynechococcus elongatus* as a well characterised[33,34], highly active and relatively robust **PSII** variant[35,36]. Loadings of 24 $\pm$ 4 nmol cm^{-2} and 143 $\pm$ 25 pmol cm^{-2} were determined by inductively-coupled plasma optical emission spectroscopy (ICP-OES) and Ultraviolet-Visible (UV-Vis) spectrophotometry for **P$_{Os}$** and **PSII**, respectively (**Supplementary Fig. 4**). The redox polymer **P$_{Os}$** mediates electron transfer between **PSII** and the IO-TiO$_2$|**dpp** surface, enhancing their electrical connection, and physically stabilises **PSII** on the electrode[4,37]. The integration of all biotic and abiotic components in the hybrid photoanode was further confirmed by high angular annular dark field scanning transmission electron microscopy (HAADF-STEM) (**Supplementary Fig. 5**).

The UV-Vis absorption spectra of **dpp**, **P$_{Os}$** and **PSII** in solution and individually adsorbed on IO-TiO$_2$ electrodes were recorded (**Fig. 1** and **Supplementary Fig. 6**). IO-TiO$_2$|**PSII** displays absorption maxima (λ_{max}) at 450 nm (B$_{x/y}$ Soret bands) and 680 nm (Q$_y$ band)[38], whereas IO-TiO$_2$|**dpp** showed a broad absorption from 475 to 575 nm. Thus, the absorption spectra of the co-sensitised IO-TiO$_2$ electrode demonstrate panchromatic light absorption and highlight the light harvesters' complementarity desired for a semi-artificial Z-scheme. For comparison, the spectrum of **RuP** (λ_{max} = 457 nm) significantly overlaps with **PSII** (λ_{max} of B$_{x/y}$ band at 450 nm). The IO-TiO$_2$|**P$_{Os}$** spectrum consisted of a broad and weak absorption, in line with the modest molar absorption of **P$_{Os}$** (ε = 8.72 mM^{-1} cm^{-1} at 531 nm)[4], which is not expected to

substantially affect light conversion efficiency in the fully assembled IO-TiO$_2$|**dpp**|**P$_{Os}$**−**PSII** tandem system.

Photoelectrochemistry

The photocurrent response (*J*) of IO-TiO$_2$|**dpp**|**P$_{Os}$**−**PSII** was recorded by PF-PEC at an applied potential (*E$_{app}$*) in a three-electrode configuration. Stepped-potential chronoamperometry under periodic illumination with UV-filtered simulated solar light was used (1.5 AM filter; irradiance *E$_e$* = 100 mW cm^{-2}; λ > 420 nm, **Fig. 2**). Photogenerated electrons in **PSII** are transferred to the electron acceptor plastoquinone B (Q$_B$) (**Fig. 1**)[9]. The holes are collected at the oxygen-evolving complex (OEC), where water is oxidised to liberate protons and gaseous O$_2$. The conduction band (CB) of IO-TiO$_2$ receives electrons from the photoexcited **dpp** which is thereby oxidised (**dpp$^+$**), giving rise to anodic photocurrent. The Os^{2+}-complex embedded in **P$_{Os}$** mediates the electrons between reduced Q$_B$ and oxidised **dpp** to close the electric circuit between the two light absorbers.

The photoanodic current onset potential (*E$_{onset}$*) of approximately −0.5 V vs. standard hydrogen electrode (SHE) is consistent with the reported anatase TiO$_2$ conduction band (CB) edge of approximately −0.6 vs. SHE[39] (**Fig. 2; Supplementary Fig. 7**). The IO-TiO$_2$|**dpp**|**P$_{Os}$**−**PSII** tandem electrode exhibits a shift of more than 0.5 V towards negative potential compared to single-absorber photoanodes with immobilised **PSII**[3,4,40], which makes it a promising candidate for bias-free overall water splitting. Potential independent steady-state photocurrents (80 μA cm^{-2}) were observed at *E$_{app}$* > −0.2 V vs. SHE (**Fig. 2b**) and attributed to water oxidation[3,4]. Prolonged irradiation at *E$_{app}$* > −0.2 V vs. SHE results in an irreversible drop in photocurrent, most likely due to **PSII** photodegradation (irreversible light-induced D1 subunit damage)[4].

Control experiments omitting one component of the tandem photoanode exhibited only a marginal photoactivity. The small background photoresponse for IO-TiO$_2$|**dpp**|**PSII** and IO-TiO$_2$|**dpp**|**P$_{Os}$** (**Fig. 2**, and similar for IO-TiO$_2$|**dpp**, **Supplementary Fig. 7a,b**) can be assigned to stoichiometric electron transfer from photoexcited **dpp** (**dpp***) to TiO$_2$ without regeneration and photocatalytic turnover of the dye. Low photocurrent in the absence of **P$_{Os}$** (IO-TiO$_2$|**dpp**|**PSII**) supports insufficient direct electronic interaction between **PSII** and **dpp** without the redox polymer[4]. No significant photocurrents were observed in the absence of **dpp** (IO-TiO$_2$|**P$_{Os}$**–**PSII**, **Fig. 2**, IO-TiO$_2$, IO-TiO$_2$|**P$_{Os}$**, IO-TiO$_2$|**PSII**, **Supplementary Fig. 7a,b**) consistent with the more positive reduction potentials of **PSII**'s Q$_B$ and **P$_{Os}$** relative to the CB of TiO$_2$, resulting in unfavourable electron transfer. The presented semi-artificial system therefore demonstrates the successful assembly of a functional biotic-abiotic interface for controlled electron-transfer in an artificial Z-scheme. A **PSII** tandem system based on IO-TiO$_2$|**RuP** was also assembled and exhibited a similar behaviour (**Supplementary Fig. 7c,d**). To maximise the performance of the tandem systems, screening of dye loading (**Supplementary Fig. 8**), **P$_{Os}$**/**PSII** ratio (**Supplementary Fig. 9**) and IO-TiO$_2$ thickness (**Supplementary Fig. 10**) was conducted.

Photocurrent action spectrum

The photocurrent response as a function of irradiation wavelength (the photocurrent action spectrum) was recorded for IO-TiO$_2$|dye|**P$_{Os}$**–**PSII** and relevant control samples (**Fig. 3a**) to characterise the complementary light absorption of the tandem photoanode (**Supplementary Fig. 1**). In a typical experiment, the wavelength was decreased from 760 to 420 nm (λ_{scan}) at E_{app} = 0.5 V vs. SHE whilst measuring the

photocurrent. The action spectra were corrected to equal photon flux at each wavelength and normalised (**Supplementary Figs. 11, 12**).

In agreement with the photocurrent responses under full visible light irradiation (**Fig. 2**), IO-TiO$_2$, IO-TiO$_2$|**P$_{Os}$**, IO-TiO$_2$|**PSII** and IO-TiO$_2$|**P$_{Os}$**–**PSII** gave negligible photocurrents upon monochromatic light illumination across all wavelengths (**Fig. 3a**). **PSII**-free electrodes loaded with **dpp** (IO-TiO$_2$|**dpp**, IO-TiO$_2$|**dpp**|**P$_{Os}$**) gave small photocurrent responses concurrent with the absorption spectrum of **dpp**, consistent with the assignment of background current due to **dpp** photooxidation (see above). For the functional IO-TiO$_2$|**dpp**|**P$_{Os}$**–**PSII** tandem system, the photocurrent onset was observed at λ_{scan} = 620 nm, with a maximum photocurrent at approximately 560 nm. This photoresponse is consistent with the spectral overlap of **PSII** with **dpp** and the required simultaneous excitation of both photoactive components[41]. The absence of photocurrent at λ_{scan} > 620 nm is consistent with the requirement of **dpp** excitation for electron injection into the CB of TiO$_2$ and **P$_{Os}$** oxidation. An external quantum efficiency (EQE)[21] of 2.7% was obtained at λ_{max} = 560 nm (E_e = 6 mW cm^{-2}).

Dual-wavelength action spectra were also recorded by coupling excitation by the scanned monochromatic light (λ_{scan}) to simultaneous irradiation at a fixed wavelength to continuously excite either **PSII** (λ_{const} = 660 nm, **Fig. 3b** and **Supplementary Fig. 12b**) or **dpp** (λ_{const} = 523 nm, **Supplementary Fig. 12c**). Continuous excitation of **PSII** (thereby probing **dpp**) in IO-TiO$_2$|**dpp**|**P$_{Os}$**–**PSII** (**Fig. 3b**) led to an action spectrum profile (with regard to λ_{scan}) similar to the UV-Vis spectrum of **dpp** and the single-wavelength excitation experiment. In comparison to the latter, a maximum at λ_{scan} = 550 nm was also observed, but with a 40% higher photocurrent magnitude. The overall photocurrent cross-section using dual-

excitation (**Fig. 3b**) was approximately two times higher compared to cross-sections of individual components (**Fig. 3a**), confirming the functional and efficient dual-absorber tandem mechanism in the IO-TiO$_2$|**dpp**|**P$_{Os}$**−**PSII** (**Supplementary Fig. 1**).

Continuous excitation of **dpp** (probing **PSII**) (**Supplementary Fig. 12c**) resulted in a general increase in photocurrent across all wavelengths (760 to 420 nm) compared to the single-wavelength excitation action spectrum. A new photocurrent maximum was detected at 680 nm, corresponding to the **PSII** Q$_y$ band. A photocurrent maximum at 550 nm remained, corresponding to higher intensity excitation of the **PSII**/**dpp** spectral overlap region, leading to higher photocurrent compared to the single-wavelength experiment. Absorption at 480 nm, corresponding to excitation of the **PSII** β-carotene, and ≤ 420 nm, corresponding to excitation of the B$_x$ and B$_y$ bands, were also observed. Action spectra of the **RuP**-sensitised photoanodes recorded for comparison (**Supplementary Fig. 13, 14**) also correlated with the UV-Vis absorption spectrum of **RuP** (**Supplementary Fig. 6**) and exhibited analogous features.

Bias-free overall water splitting via artificial Z-scheme

The negative E_{onset} and broad absorption spectrum of the IO-TiO$_2$|**dpp**|**P$_{Os}$**−**PSII** tandem photoanode make it a suitable light absorber for bias-free (unassisted) overall water splitting. To achieve this long-standing goal[16,42], the photoanode was wired to a previously reported indium tin oxide (ITO)-based IO-ITO|**H$_2$ase** cathode[3], which utilises a reversible biological electrocatalyst for H$_2$ production integrated in a hierarchically-structured ITO electrode. The *Desulfomicrobium baculatum* **[NiFeSe]-H$_2$ase** was used for its high proton reduction activity, O$_2$ tolerance under reductive conditions and marginal inhibition by H$_2$, offering advantageous properties for water splitting compared to O$_2$-sensitive **[FeFe]-H$_2$ases** available in algal H$_2$ production[43].

11

ITO has been shown to be a suitable electrode material for the wiring of **[NiFeSe]-H₂ases** in a direct electron transfer regime, and the IO-ITO|**H₂ase** electrode exhibited high current densities for proton reduction (> 400 μA cm^{-2}) and E_{onset} of −0.35 V vs. SHE (pH 6.5; N₂ atmosphere)[3]. Comparison of the voltammetric responses of IO-TiO₂|**dpp**|**P$_{Os}$**–**PSII** and IO-ITO|**H₂ase** measured individually (**Supplementary Fig. 15**) indicate that E_{onset} of the anodic (−0.50 V vs. SHE) and cathodic (−0.35 V vs. SHE) current responses overlap by approximately 0.15 V[42,44]. Thus, a two-electrode PEC cell consisting of the two enzyme-modified electrodes should be capable of bias-free solar-driven water splitting, assuming only minor resistive solution/membrane losses[45]. Comparison of the current densities indicates that IO-TiO₂|**dpp**|**P$_{Os}$**–**PSII** should primarily limit the current response when wired to IO-ITO|**H₂ase**.

A semi-artificial PEC device was therefore assembled consisting of a IO-TiO₂|**dpp**|**P$_{Os}$**–**PSII** photoanode connected to a IO-ITO|**H₂ase** cathode separated by a glass frit membrane in a two-electrode, two-compartment cell. **Fig. 4** demonstrates the ability of the system to achieve bias-free solar-driven water splitting. Chronoamperometry measurements with longer irradiation times (**Fig. 4a**) were performed to minimise the charging effects below an applied voltage (U_{app}) of 0 V. At more positive voltages, the charging effects were decreased and photocurrent responses stabilised. Upon irradiation with UV-filtered simulated solar light, a current density of 28 ± 5 μA cm^{-2} was achieved at U_{app} = 0 V (**Fig. 4b**). Voltage independent steady-state photocurrents (122 ± 21 μA cm^{-2}) were reached at U_{app} = 0.3 V. The photocurrent magnitudes were similar to a two-electrode system with a Pt cathode instead of IO-ITO|**H₂ase** (**Supplementary Fig. 16**), consistent with photocurrent limitation by IO-TiO₂|**dpp**|**P$_{Os}$**–**PSII**. A two-electrode system with a IO-TiO₂|**H₂ase**

cathode was also assembled and exhibited a similar behaviour, albeit with less charging due to the matched Fermi levels of IO-TiO$_2$ (**Supplementary Fig. 17**).

Overall water splitting with the IO-TiO$_2$|**dpp**|**P$_{Os}$**–**PSII** || IO-ITO|**H$_2$ase** PEC cell was studied at U_{app} = 0.0 and 0.3 V (**Supplementary Figure 18a**). At zero bias (U_{app} = 0 V), the initial photocurrent decayed from 130 µA cm^{-2} to 5 µA cm^{-2} after 1 h irradiation, leading to an average half-life time ($\tau_{1/2}$) of 6.5 min. At U_{app} = 0.3 V, the photocurrent decayed from 140 µA cm^{-2} to 15 µA cm^{-2} after 1 h irradiation with a $\tau_{1/2}$ of ~8 min. These lifetimes are similar to previously reported **PSII**-based photoanodes[3,4], and consistent with the stability of **PSII** *in vivo* ($\tau_{1/2}$ of ~20 min)[9]. The relative stability of the IO-TiO$_2$|**dpp**|**P$_{Os}$**–**PSII** system can be attributed to the efficient electron transfer between TiO$_2$–**dpp**–**P$_{Os}$**–**PSII**, physical stabilisation of **PSII** by the polymer and reduced accumulation of excited states in Chl *a* within **PSII**[46]. However, it is important to emphasise that the current hybrid enzyme system is a proof-of-concept device, and its practical applicability is intrinsically limited by the photodegradation pathways of **PSII** *in vitro*.

After 1 h of continuous light irradiation at U_{app} = 0.0 V, H$_2$ was detected (0.06 µmol H$_2$ cm^{-2}) with a Faradaic efficiency (η_F) of 76%, but reliable O$_2$ analysis was prevented by the detection limit of the apparatus. At U_{app} = 0.3 V, O$_2$ and H$_2$ were quantified (**Fig. 4b, inset**) with η_F of 88 ± 12% and 82 ± 10%, respectively (**Supplementary Table 1**) and a STH conversion efficiency of 0.14 ± 0.02 % was obtained[47]. A **PSII**-based TOF of 2.5 ± 0.3 mol O$_2$ (mol **PSII**)$^{-1}$ s^{-1} was calculated based on quantified O$_2$ and **PSII**[3,4]. Previously, similar η_F values were reported for benchmark **PSII**-photoanodes: diffusional-mediated IO-ITO|**PSII**[3] and IO-ITO|**P$_{Os}$**–**PSII**[4], but required significantly higher driving force (U_{app} = 0.9 V and E_{app} = 0.5 V vs. SHE, respectively). Negligible photocurrents were detected in control experiments (**Supplementary Fig. 18b**;

Supplementary Table 1). O$_2$ evolution was also confirmed using a rotating ring-disc electrode (RRDE) setup (**Supplementary Fig. 19**).

Conclusions

The reported enzyme-based tandem PEC system consisting of an IO-TiO$_2$|**dpp**|**P$_{Os}$**–**PSII** photoanode connected to a IO-ITO|**H$_2$ase** cathode achieves the long-standing goal of a bias-free *in vitro* system for overall water splitting using **PSII** (O$_2$ generation) connected to **H$_2$ase** (H$_2$ generation). This semi-artificial design addresses key limitations in biology as PEC wiring of **PSII** to **H$_2$ase** via an abiotic dye allows for: panchromatic solar light absorption by using a synthetic green-light absorber (in contrast to non-complementary absorption by **PSI**); quantitative use of electrons extracted from **PSII** for H$_2$ production (and thereby avoiding inefficient metabolic pathways); and separation of H$_2$ and O$_2$ gas in separate compartments (as opposed to inhibiting an O$_2$-sensitive **H$_2$ase**).

The tandem system produced H$_2$ and O$_2$ from water with high Faradaic efficiencies in 2:1 ratio and presents an effective strategy for constructing biotic-abiotic interfaces. Future work will involve investigating other dyes and replacing TiO$_2$ with a semiconductor with a more negative CB potential to enhance driving force for more efficient catalysis or CO$_2$ reduction chemistry. Moreover, our study provides a blueprint for advancing future semi-artificial systems capable of bias-free photocatalysis and a toolbox for developing proof-of-concept model systems for solar energy conversion.

Materials and Methods

Materials

All chemicals: 2-(N-morpholino)ethane sulfonic acid (MES, Alfa Aesar), tetrabutylammonium hydroxide (TBAOH, Sigma Aldrich), $CaCl_2$ (Breckland Scientific), $MgCl_2$ (Fisher Scientific), KCl (Alfa Aesar), KOH (Breckland Scientific), polystyrene (PS) beads (Polysciences Inc., 750 nm diameter, 2.6 % w/v suspension in H_2O), titanium dioxide (TiO_2) nanoparticles (NPs) (Evonik Industries, Aeroxide® P25 TiO_2 nanoparticles; 21 nm diameter; 80/20 anatase/rutile w/w), indium tin oxide (ITO) NPs (Sigma Aldrich; <50 nm diameter), fluorine-doped tin oxide (FTO) coated glass slides (8 Ω sq^{-1}; Sigma Aldrich) and Parafilm® (Sigma Aldrich) were purchased from commercial suppliers and used without further purification unless otherwise noted. Methanol, absolute ethanol, 2-propanol, dimethyl sulfoxide, tetrahydrofuran (HPLC grade) were purchased from Sigma Aldrich. **PSII** was isolated from the thermophilic cyanobacterium *Thermosynechococcus elongatus* according to a previously reported procedure[35], with an average oxygen-evolving activity of approximately 5,300 µmol O_2 h^{-1} mg^{-1} of chlorophyll *a* (Chl *a*). A stock **PSII** solution containing 2.6 mg Chl *a* mL^{-1} (83 µM **PSII**) was stored in a liquid N_2 Dewar. **[NiFeSe]-H₂ase** from *Desulfomicrobium baculatum* was purified using a previously published method[48], with a specific activity of 2,115 µmol H_2 min^{-1} mg^{-1}. Stock solutions of **H₂ase** (8 µM, in 20 mM Tris/HCl buffer, pH 7.0) were stored in 10-20 µL aliquots at −40 °C in an anaerobic glovebox and used immediately after thawing.

Polymer and dye synthesis

Poly(1-vinylimidazole-*co*-allylamine)-Os(bipy)₂Cl (**P$_{Os}$**)[37] was synthesised according to previously reported procedures[4]. In brief, an ethanolic solution of *cis*-[OsCl₂(bipy)₂] and poly(1-vinylimidazole-*co*-allylamine) backbone (1/1.65 weight ratio) was stirred for

5 days at 90 °C. **P$_{Os}$** was then precipitated by addition of diethyl ether, collected by centrifugation and dried under vacuum to obtain a reddish powder. An aqueous solution of **P$_{Os}$** (10 mg mL^{-1}) was used in all experiments. The diketopyrrolopyrrole-based dye (**dpp**) was synthesised using a previously reported procedure[27]. Briefly, pseudo-Stobbe condensation of 1-bromo-4-cyanobenzene with diethyl succinate was followed by lactam N-alkylation then desymmetrisation of the intermediate via Suzuki–Miyaura cross-coupling. The phosphonic acid anchoring group was then added via Hirao cross-coupling using diethyl phosphite followed by hydrolysis. To obtain ruthenium bis(2,2'-bipy)(4,4'-bis(phosphonic acid)-2,2'-bipy) dibromide (**RuP**), Me$_3$SiBr was added to a solution of [Ru(bipy)$_2$(4,4'-(PO$_3$Et$_2$)$_2$bipy)](PF$_6$)$_2$ in dry dimethylformamide and the mixture was heated in the dark at 60 °C for 18 h under Ar then concentrated under vacuum. Methanol was added and the solution was stirred at room temperature for 3 h. The product was precipitated by adding diethyl ether and dried under vacuum to afford [Ru(bipy)$_2$(4,4'-(PO$_3$H$_2$)$_2$bipy)](Br)$_2$ (**RuP**)[29]. Both **dpp** and **RuP** were characterised as previously reported.

Instrumentation

The surface morphology of the electrodes was analysed by scanning electron microscopy (SEM; Philips SFEG XL30; acceleration voltage 5 kV; WD 5 mm), energy dispersive X-ray (EDX) spectroscopy attached to the SEM, scanning transmission electron microscopy (STEM; TitanX 60-300 with High Angle Annular Dark Field (HAADF) detector; acceleration voltage 300 kV) and powder X-Ray diffraction (PXRD; PANalytics Empyrean 2). A centrifuge (5804 Eppendorf), furnace (Carbolite, ELF 11/14B/301) and UV/Ozone cleaner (ProCleaner Plus, BioForce Nanosciences) were used for electrode preparation. UV-vis absorption spectra were recorded on an FS5 spectrofluorometer (Edinburgh Instruments; integrating sphere reflectance mode) and

spectrophotometer (Varian Cary 50, Agilent), using cuvettes with an optical path length of 1 cm (transmittance mode). With the integrating sphere, the measurement was performed by concentrating the light reflected from the electrode on the detector using a polytetrafluoroethylene-coated sphere (120 mm in diameter). The relative reflectance was measured with respect to the reflectance of the reference standard white board, which is taken to be 100%.

Preparation of IO-TiO$_2$ electrodes

The IO-TiO$_2$ electrodes were fabricated according to a method adopted from a previously reported procedure for the synthesis of IO-ITO[3,4]. FTO-coated glass slides (2 x 1 cm^2) were cleaned by sonication in two 30 min steps in 2-propanol and absolute ethanol. First, to ensure no direct contact of the electroactive components (**PSII** and **P$_{Os}$**) with the FTO layer, it was coated with a layer of mesoporous TiO$_2$ (mesoTiO$_2$). TiO$_2$ NPs (50 mg) were dispersed via sonication for 20 min in a MeOH/water mixture (300 µL, 5:1 v/v). The suspension (10 µL) was deposited onto a 0.50 cm^2 area defined by a Parafilm® ring on an FTO slide and doctor bladed to give a 3 µm thick mesoTiO$_2$ layer. The IO-TiO$_2$ layer was then deposited on top of the mesoTiO$_2$ layer. TiO$_2$ NPs (30 mg) were dispersed in a water/MeOH mixture (300 µL, 4:1 v/v) via sonication (3 h). The PS bead dispersion (1 mL) was centrifuged (10,000 rpm, 3 min), and the supernatant was removed. The pellet was redispersed in MeOH (1 mL) before being centrifuged again (10,000 rpm, 0.5 min). The supernatant was removed and the TiO$_2$ NPs dispersion was added to the PS pellet. The pellet was dispersed into the solution by sonication (10 min, <10 °C). The resulting PS-TiO$_2$ NPs dispersion was drop-cast (5 µL) onto a 0.25 cm^2 area defined by a Parafilm ring on an FTO slide. Following evaporation of the solvent, the electrodes were annealed at a 1 ^{0}C min^{-1} ramp rate from room temperature to 500 ^{0}C and sintered for 20 min giving a 20 µm thick IO-TiO$_2$ film. The electrodes were allowed to cool to room temperature and cleaned with an

UV/ozone cleaner (15 min) and characterised by SEM and HAADF-STEM, elemental mapping using EDX, and powder XRD (**Supplementary Fig. 2**).

Preparation of IO-TiO$_2$|dye electrodes

IO-TiO$_2$ electrodes with a pore diameter of 750 nm, 20 μm film thickness and a geometrical surface area of 0.25 cm^2 were used in all experiments, unless stated otherwise. The IO-TiO$_2$|dye modified electrodes were prepared by soaking IO-TiO$_2$ electrodes in solutions of **dpp** or **RuP** (0.15 mM in THF/H$_2$O, respectively) overnight in the dark. To remove excess dye prior to enzyme/polmer deposition, the IO-TiO$_2$|**dpp** electrodes were rinsed with THF, followed by water, then air-dried. Similarly, the IO-TiO$_2$|**RuP** electrodes were rinsed with water and air-dried.

Preparation of IO-TiO$_2$|dye|P$_{Os}$-PSII electrodes

The IO-TiO$_2$|dye|**P$_{Os}$**–**PSII** electrodes were prepared by depositing a blend of **PSII** (1 μL, 2.6 mg Chl a mL^{-1}) stock solution and **P$_{Os}$** (1 μL, 10 mg mL^{-1}) onto the IO-TiO$_2$|dye electrode (20 μm thick) and incubating the electrodes in the dark for 15 min at room temperature. Prior to electrochemical studies, the IO-TiO$_2$|dye|**P$_{Os}$**–**PSII** electrode was rinsed (3 × 500 μL) with the **PSII** buffer electrolyte solution (composition given below) to remove loosely bound species from the electrode surface.

Determination of PSII, P$_{Os}$ and dye loading on IO-TiO$_2$

The amount of **PSII** on the IO-TiO$_2$ surface was quantified by scratching off the IO-TiO$_2$ from the FTO glass substrate and washing it with MeOH (500 μL) to extract Chl a (originating from **PSII**) from the electrode surface into a centrifuge vial. The vial was centrifuged (10,000 rpm, 1 min), and the UV-vis spectrum of the supernatant was recorded (**Supplementary Fig. 4b**). The band with an absorption maximum of λ_{max} = 665 nm assigned to Chl a (extinction coefficient ε = 79.95 (Chl a mg)$^{-1}$ mL cm^{-1})[49]

was used to calculate the amount of **PSII** monomers[49] assuming 35 Chl *a* molecules

per **PSII** monomer[33]. The Os-complex loading in the **P$_{Os}$** was determined by ICP-OES

obtained by washing off the **P$_{Os}$** from the IO-TiO$_2$ electrode with aqueous concentrated

HNO$_3$ solution (70% wt) and measuring the concentration of the Os^{2+} metal ions

relative to Os ICP standard (1 mg Os mL^{-1} in 20% HCl, Ricca Chemical). The **dpp/RuP**

loadings were quantified by scratching off the IO-TiO$_2$|dye from the glass substrate

and washing with TBAOH (0.1 M) in MeOH (500 µL) to extract the dye from the

electrode surface into a centrifuge vial. The vial was centrifuged (10,000 rpm, 1 min)

and the UV-vis spectrum of the supernatant was recorded (**Supplementary Fig. 4a**).

The amount of dye desorbed into solution was estimated using the Beer-Lambert Law

(**Supplementary Fig. 4c,d**).

Preparation of IO-ITO|H$_2$ase electrodes

[NiFeSe]-H$_2$ase was immobilised on ozone cleaned IO-ITO electrodes (20 µm film

thickness, geometrical surface area, *A* = 0.25 cm^2) by depositing the enzyme solution

(5 µL) on the electrode surface, followed by incubation for approximately 5 min. The

loading of **[NiFeSe]-H$_2$ase** (40 pmol) was adjusted to the electrode thickness, as

reported previously[3].

Protein film photoelectrochemistry (PF-PEC) measurements

Chronoamperometry and cyclic voltammetry (CV) measurements were performed

using an Ivium Compactstat potentiostat and a gas-tight two-compartment glass cell

with a water jacket for temperature control (T = 25 °C). A three-electrode setup was

employed with an IO-TiO$_2$ (or IO-ITO) working electrode, a Ag/AgCl (3 M KCl)

reference electrode and a Pt wire counter electrode separated by a glass frit in another

compartment. The cell was filled with a **PSII** electrolyte solution (12 mL, pH 6.5)

consisting of CaCl$_2$ (20 mM), MgCl$_2$ (15 mM), KCl (50 mM). All current densities (µA

cm^{-2}) are reported with respect to the geometrical surface area of the electrodes. Experimentally measured potentials are reported vs. SHE using the conversion E_{SHE} = $E_{Ag/AgCl}$ + 0.197 V (25 °C).

Bias-free PEC overall water splitting and O_2 and H_2 quantification was studied using a two-electrode configuration with an IO-TiO$_2$ photoanode containing **PSII** and an IO-ITO|**H$_2$ase** cathode. In all experiments involving IO-ITO|**H$_2$ase** cathode, MES (40 mM) was added to the **PSII** electrolyte solution as it was found to retain **H$_2$ase** electroactivity and only caused negligible photocurrents from MES oxidation.

PEC experiments were performed using a Xe lamp (150 W, Newport) Solar Light Simulator (LOT Quantum Design, light intensity flux (irradiance) (E_e) 100 mW cm^{-2}, AM 1.5G filter, λ > 420 nm filter). Action spectra were recorded with a Xe lamp (300 W, Newport) Solar Light Simulator (LOT Quantum Design) coupled to a monochromator (MSH300, LOT Quantum Design). For dual excitation experiments, an Ivium modulight LED module (λ = 460/523/660 nm; 4 mW cm^{-2}) was used as a second light source. Light intensity was measured as a function of wavelength with a thermal sensor (S302C, Thorlabs) and power meter console (PM100D, Thorlabs)

IO-TiO$_2$|dye|**P$_{Os}$**–**PSII** electrodes were exposed to dark and light cycles in the PF-PEC measurements. The photocurrent response was defined as the baseline-corrected (dark current-subtracted) photocurrent peak shoulder edge after a light exposure, to avoid overestimation of photocurrent[9]. Action spectra were corrected to equal photon flux at each wavelength and normalised (taking the peak at 500 nm as unity). Error bars are ± sample standard deviation estimated from at least three experiments. All data processing was performed using OriginPro 9.1 software.

RRDE experiments were performed using Ag/AgCl (3 M KCl) reference and glassy carbon counter electrodes. The disk/ring apparatus was embedded in a cylindrical polyether ether ketone housing. A Pt ring electrode surrounded a glassy carbon disk electrode on which a mesoporous TiO_2 layer was deposited prior to depositing additional components (**dpp**, **P_{Os}**, **PSII**). The electrodes were placed in a single-compartment cell under continuous purging with N_2. The ring-disk electrode was rotated at 400 rpm for O_2 evolution measurements and the collection efficiency of the ring electrode was calibrated under conditions similar to those of the experiment (**Supplementary Fig. 19**).

Product analysis

Quantification of O_2 was performed using a fluorescence-based O_2 sensor (Neofox; Ocean Optics FOSFOR-R probe) inside an anaerobic glovebox (Belle Technology) to avoid ingress of atmospheric O_2. The probe was placed inside the anodic compartment headspace of a two-compartment cell, protected from direct irradiation. The results are reported as the average of six measurements and the background signal was subtracted from all measurements. The reported O_2 values were corrected for dissolved O_2 using Henry's Law ($K_H(O_2)$) = 769.23 L atm mol^{-1} at 25 °C). H_2 was analysed by taking aliquots of the headspace gas (50 µL) after electrolysis and quantified using gas chromatography (GC; Agilent 7890, carrier gas N_2, flow rate 0.7 mL min^{-1}, molecular sieve column, thermal conductivity detector). Calibration runs were performed to quantify the volume of H_2 evolved. The reported Faradaic efficiencies were corrected by subtracting the **dpp** dye background current estimated from control experiments from the experimental data.

Data availability

The data that support the presented plots within this paper and other findings of this study are available at the University of Cambridge data repository with the identifier https://doi.org/xxxxx.

References

1. Sakimoto, K. K., Wong, A. B. & Yang, P. Self-photosensitization of nonphotosynthetic bacteria for solar-to-chemical production. *Science* **351,** 74–77 (2016).

2. Yehezkeli, O. *et al.* Integrated photosystem II-based photo-bioelectrochemical cells. *Nat. Commun.* **3,** 742–747 (2012).

3. Mersch, D. *et al.* Wiring of Photosystem II to Hydrogenase for Photoelectrochemical Water-splitting. *J. Am. Chem. Soc.* **137,** 8541–8549 (2015).

4. Sokol, K. P. *et al.* Rational wiring of photosystem II to hierarchical indium tin oxide electrodes using redox polymers. *Energy Environ. Sci.* **9,** 3698–3709 (2016).

5. Ort, D. R. *et al.* Redesigning photosynthesis to sustainably meet global food and bioenergy demand. *Proc. Natl. Acad. Sci.* **112,** 8529–8536 (2015).

6. Tachibana, Y., Vayssieres, L. & Durrant, J. R. Artificial photosynthesis for solar water-splitting. *Nat. Photonics* **6,** 511–518 (2012).

7. Woolerton, T. W., Sheard, S., Chaudhary, Y. S. & Armstrong, F. A. Enzymes and bio-inspired electrocatalysts in solar fuel devices. *Energy Environ. Sci.* **5,** 7470–7490 (2012).

8. Léger, C. & Bertrand, P. Direct Electrochemistry of Redox Enzymes as a Tool for Mechanistic Studies Direct Electrochemistry of Redox Enzymes as a Tool for Mechanistic Studies. *Chem. Rev.* **108,** 2379–2438 (2008).

9. Kato, M., Zhang, J. Z., Paul, N. & Reisner, E. Protein film photoelectrochemistry of the water oxidation enzyme photosystem II. *Chem. Soc. Rev.* **43,** 6485–6497 (2014).

10. Bard, A. J. & Fox, M. A. Artificial Photosynthesis: Solar Splitting of Water to Hydrogen and Oxygen. *Acc. Chem. Res.* **28,** 141–145 (1995).

11. Govindjee, Shevela, D. & Björn, L. O. Evolution of the Z-scheme of photosynthesis: a perspective. *Photosynth. Res.* **133,** 5–15 (2017).

12. Barber, J. & Tran, P. D. From natural to artificial photosynthesis. *J. R. Soc. Interface* **10,** 1–16 (2013).

13. Khetkorn, W. *et al.* Microalgal hydrogen production – A review. *Bioresour. Technol.* **243,** 1194–1206 (2017).

14. Kruse, O., Rupprecht, J., Mussgnug, J. H., Dismukes, G. C. & Hankamer, B. Photosynthesis: a blueprint for solar energy capture and biohydrogen production technologies. *Photochem. Photobiol. Sci.* **4,** 957–969 (2005).

15. Michel, H. The nonsense of biofuels. *Angew. Chem. Int. Ed.* **51,** 2516–2518 (2012).

16. Esper, B., Badura, A. & Rögner, M. Photosynthesis as a power supply for (bio-)hydrogen production. *Trends Plant Sci.* **11,** 543–549 (2006).

17. Hu, S., Xiang, C., Haussener, S., Berger, A. D. & Lewis, N. S. An analysis of the optimal band gaps of light absorbers in integrated tandem photoelectrochemical water-splitting systems. *Energy Environ. Sci.* **6,** 2984 (2013).

18. Kothe, T. *et al.* Combination of A Photosystem 1-Based Photocathode and a Photosystem 2-Based Photoanode to a Z-Scheme Mimic for Biophotovoltaic Applications. *Angew. Chem. Int. Ed.* **52,** 14233–14236 (2013).

19. Hartmann, V. *et al.* Redox hydrogels with adjusted redox potential for improved efficiency in Z-scheme inspired biophotovoltaic cells. *Phys. Chem. Chem. Phys.* **16,** 11936–11941 (2014).

20. Kim, Y. *et al.* Hybrid Z-Scheme Using Photosystem I and $BiVO_4$ for Hydrogen Production. *Adv. Funct. Mater.* **25,** 2369–2377 (2015).

21. Rao, K. K. *et al.* Photoelectrochemical responses of photosystem II particles immobilized on dye-derivatized TiO_2 films. *J. Photochem. Photobiol. B* **5,** 379–389 (1990).

22. Wang, W. *et al.* Spatially Separated Photosystem II and a Silicon Photoelectrochemical Cell for Overall Water Splitting : A Natural–Artificial Photosynthetic Hybrid. *Angew. Chem. Int. Ed.* **8530,** 9229–9233 (2016).

23. Pinhassi, R. I. *et al.* Hybrid bio-photo-electro-chemical cells for solar water splitting. *Nat. Commun.* **7,** 1–10 (2016).

24. O'Regan, B. & Grätzel, M. A low-cost, high-efficiency solar cell based on dye-sensitised colloidal TiO_2 films. *Nature* **353,** 737–740 (1991).

25. Xu, P., McCool, N. S. & Mallouk, T. E. Water splitting dye-sensitized solar cells. *Nano Today* **14,** 42–58 (2017).

26. Warnan, J. *et al.* A compact diketopyrrolopyrrole dye as efficient sensitizer in titanium dioxide dye-sensitized solar cells. *J. Photochem. Photobiol. A Chem.* **226,** 9–15 (2011).

27. Warnan, J. *et al.* Solar H_2 evolution in water with modified diketopyrrolopyrrole dyes immobilised on molecular Co and Ni catalyst–TiO_2 hybrids. *Chem. Sci.* **8,** 3070–3079 (2017).

28. Muresan, N. M., Willkomm, J., Mersch, D., Vaynzof, Y. & Reisner, E. Immobilization of a molecular cobaloxime catalyst for hydrogen evolution on a mesoporous metal oxide electrode. *Angew. Chem. Int. Ed.* **51,** 12749–12753 (2012).

29. Lakadamyali, F., Reynal, A., Kato, M., Durrant, J. R. & Reisner, E. Electron Transfer in Dye-Sensitised Semiconductors Modified with Molecular Cobalt Catalysts : Photoreduction of Aqueous Protons. *Chem. Eur. J.* **2,** 15464–15475 (2012).

30. Knauf, R. R., Brennaman, M. K., Alibabaei, L., Norris, M. R. & Dempsey, J. L. Revealing the Relationship between Semiconductor Electronic Structure and Electron Transfer Dynamics at Metal Oxide−Chromophore Interfaces. *J. Phys. Chem. C* **117,** 25259–25268 (2013).

31. Li, F. *et al.* Immobilizing Ru(bda) Catalyst on a Photoanode via Electrochemical Polymerization for Light-Driven Water Splitting. *ACS Catal.* **5,** 3786–3790 (2015).

32. Willkomm, J. *et al.* Dye-sensitised semiconductors modified with molecular catalysts for light-driven H_2 production. *Chem. Soc. Rev.* **45,** 9–23 (2016).

33. Umena, Y., Kawakami, K., Shen, J.-R. & Kamiya, N. Crystal structure of oxygen-evolving photosystem II at a resolution of 1.9 Å. *Nature* **473,** 55–60 (2011).

34. Rapatskiy, L. *et al.* Detection of the Water-Binding Sites of the Oxygen-Evolving Complex of Photosystem II Using W‑Band ^{17}O Electron−Electron Double Resonance-Detected NMR Spectroscopy. *J. Am. Chem. Soc.* **134,** 16619–16634 (2012).

35. Kuhl, H. *et al.* Towards structural determination of the water-splitting enzyme: Purification, crystallization, and preliminary crystallographic studies of photosystem II from a thermophilic cyanobacterium. *J. Biol. Chem.* **275,** 20652–20659 (2000).

36. Kern, J. *et al.* Purification, characterisation and crystallisation of photosystem II from Thermosynechococcus elongatus cultivated in a new type of photobioreactor. *Biochim. Biophys. Acta - Bioenerg.* **1706,** 147–157 (2005).

37. Badura, A. *et al.* Photo-induced electron transfer between photosystem 2 via cross-linked redox hydrogels. *Electroanalysis* **20,** 1043–1047 (2008).

38. Senge, M. O., Ryan, A. A., Letchford, K. A., MacGowan, S. A. & Mielke, T. Chlorophylls, symmetry, chirality, and photosynthesis. *Symmetry.* **6,** 781–843 (2014).

39. Beranek, R. (Photo)electrochemical methods for the determination of the band edge positions of TiO_2-based nanomaterials. *Adv. Phys. Chem.* **2011,** 80–83 (2011).

40. Zhang, J. Z. *et al.* Competing charge transfer pathways at the photosystem II-electrode interface. *Nat. Chem. Biol.* **12,** 1046–1052 (2016).

41. Razeghifard, R. & Wydrzynski, T. J. *Artificial Photosynthesis: From Basic Biology to Industrial Application*. (John Wiley & Sons, 2007).

42. Reisner, E., Powell, D. J., Cavazza, C., Fontecilla-Camps, J. C. & Armstrong, F. A. Visible Light-Driven H_2 Production by Hydrogenases Attached to Dye-Sensitized TiO_2 Nanoparticles. *J. Am. Chem. Soc.* **131,** 18457–18466 (2009).

43. Wombwell, C., Caputo, C. A. & Reisner, E. [NiFeSe]-Hydrogenase Chemistry. *Acc. Chem. Res.* **48,** 2858–2865 (2015).

44. Hambourger, M. *et al.* [FeFe]-hydrogenase-catalyzed H_2 production in a photoelectrochemical biofuel cell. *J. Am. Chem. Soc.* **130,** 2015–2022 (2008).

45. Coridan, R. H. *et al.* Methods for comparing the performance of energy-conversion systems for use in solar fuels and solar electricity generation. *Energy Environ. Sci.* **8,** 2886–2901 (2015).

46. Cai, P. *et al.* Co-assembly of photosystem II/reduced graphene oxide multilayered biohybrid films for enhanced photocurrent. *Nanoscale* **7,** 10908–10911 (2015).

47. Dotan, H., Mathews, N., Hisatomi, T., Grätzel, M. & Rothschild, A. On the solar to hydrogen conversion efficiency of photoelectrodes for water splitting. *J. Phys. Chem. Lett.* **5,** 3330–3334 (2014).

48.   Hatchikian, E. C., Bruschi, M. & Le Gall, J. Characterisation of the Periplasmic Hydrogenase from Desulfovibrio Gigas. *Biochem. Biophys. Res. Commun.* **82,** 451–461 (1978).

49.   Porra, R. J., Thompson, W. A. & Kriedemann, P. E. Determination of accurate extinction coefficients and simultaneous equations for assaying chlorophylls a and b extracted with four different solvents: verification of the concentration of chlorophyll standards by atomic absorption spectroscopy. *Biochim. Biophys. Acta - Bioenerg.* **975,** 384–394 (1989).

Acknowledgements

Author contributions

K.P.S., W.E.R., J.Z.Z. and E.R. conceived the research. K.P.S. prepared and characterised the electrodes and performed the electrochemical experiments. W.E.R. helped with the experiment design and supported the electrochemical experiments. J.W. synthesised the **dpp** dye. N.K. carried out HAADF-STEM and RRDE measurements. M.M.N. provided the **PSII** samples. A.R. synthesised the **P$_{Os}$** polymer. K.P.S., W.E.R., N.K., J.Z.Z. and E.R. analysed the data. All authors contributed to the creation of the manuscript. E.R. supervised the work.

Supporting information

Supplementary information is available for this paper.

Reprints and permissions information is available at www.nature.com/reprints.

Correspondence and requests for materials should be addressed to E.R.

How to cite this article: Sokol, K. P. *et al.* Bias-free photoelectrochemical water splitting with photosystem II on a dye-sensitised photoanode wired to hydrogenase. *Nat. Energy* **x**, x (2018).

Competing interests

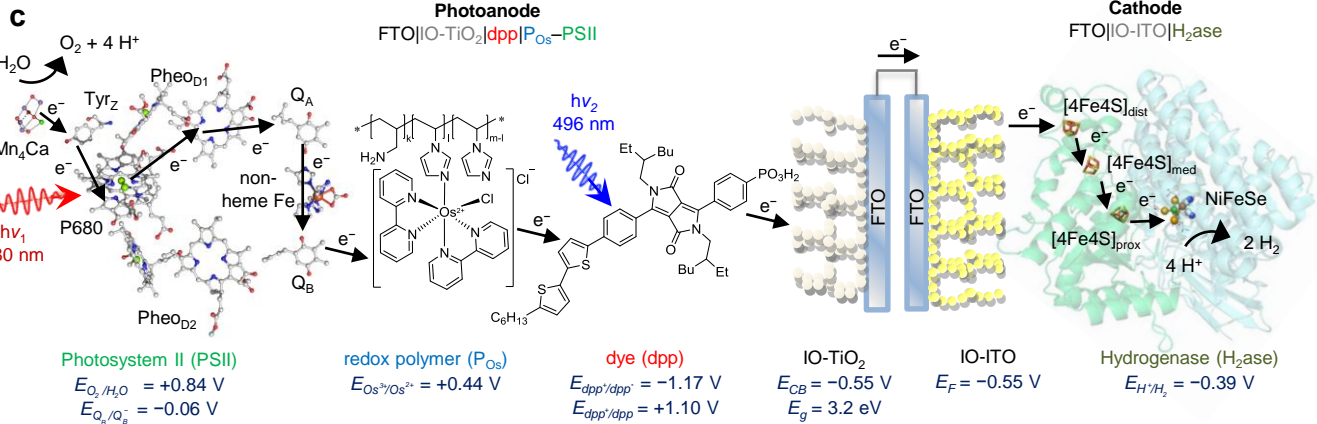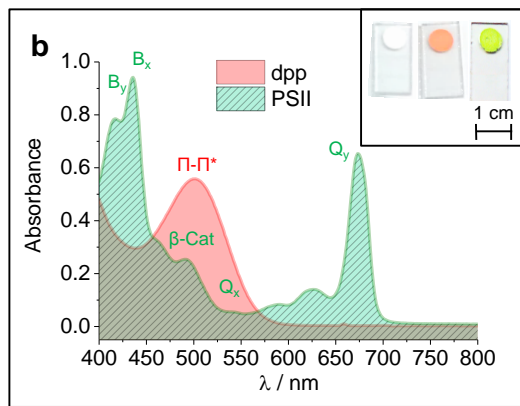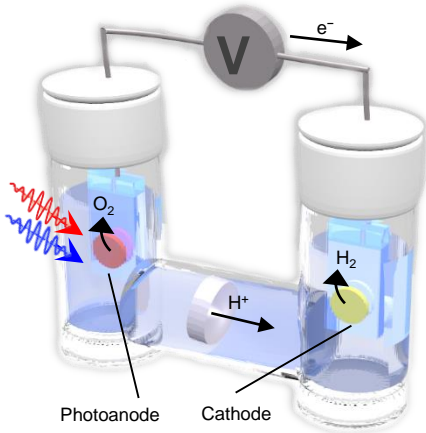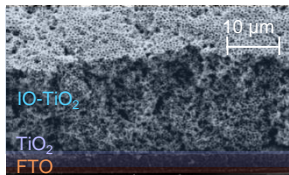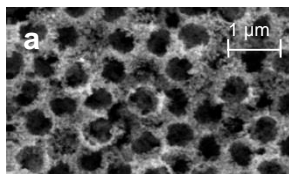The authors declare no competing interests.

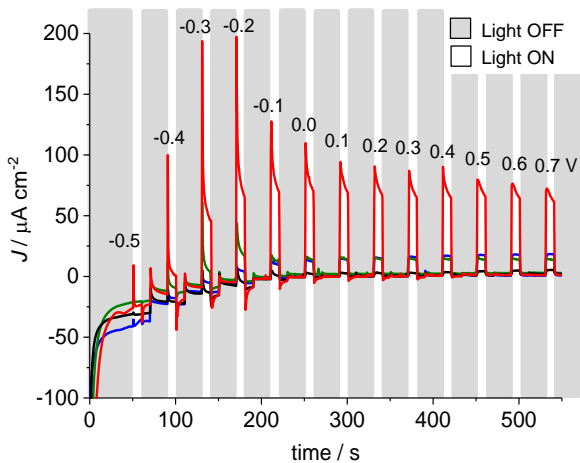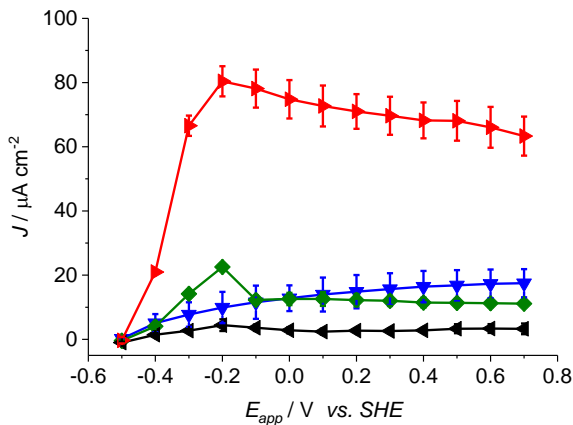**Fig. 1 | Semi-artificial tandem PEC system for unassisted overall water splitting**. **a**, Schematic representation of IO-TiO$_2$|**dpp**|polymer–**PSII** photoanode wired to IO-ITO|**H₂ase** cathode (species size not drawn to scale). SEM images of IO-TiO$_2$ photoanode architecture (top view and cross-section at 60° tilt angle). **b**, Solution UV-Vis spectra of **dpp** (0.15 µM in THF) and **PSII** (0.005 mg Chl a mL^{-1} in H$_2$O) with the photographic images of IO-TiO$_2$, IO-TiO$_2$|**dpp** and IO-TiO$_2$|**PSII**, quoting from left to right (inset). Absorptions: B$_{y/x}$, chlorophyll *a* Soret-bands; β-Cat, β-carotene; Q$_{x/y}$, chlorophyll *a* lowest-energy bands; π- π*, **dpp** π-orbital intramolecular charge transfer. **c**, Electron-transfer pathway between **PSII**, **P$_{Os}$**, **dpp**, IO-TiO$_2$, IO-ITO and **H₂ase** and the relevant redox potentials. Abbreviations: Mn$_4$Ca, oxygen-evolving complex (OEC); Tyr$_Z$, tyrosine; P680, pigment/primary electron donor; Pheo, pheophytin; Q$_A$/Q$_B$, plastoquinones; [NiFeSe], **H₂ase** active site; [4Fe4S], iron-sulphur clusters; all potentials reported vs. SHE at pH 6.5. Atom labels (**PSII**): C (grey), O (red), N (blue), Mn (violet), Ca (green), Mg (light green). Atom labels (**H₂ase**): S (yellow), Fe (brown), Ni (green), Se (light orange).

Fig. 2 | PF-PEC of tandem PSII-dye photoanode. **a**, Chronoamperometry (0.1 V potential steps with 30 s dark and 10 s light cycles) for the determination of onset potential (E_{onset}) and limiting photocurrent for IO-TiO$_2$|**dpp**|**P$_{Os}$**–**PSII** photoanode. E_{app} values (shown on top of the lines) are reported vs. SHE. Short irradiation times were used to minimise **PSII** photodegradation. **b**, Photocurrent density (J) plotted as function of E_{app} determined by stepped-potential chronoamperometry in **a**. Values of J were taken at the end of illumination (baseline-corrected for background dark current). Error bars correspond to the standard deviation (N = 3). Control experiments omitting one of the components of the tandem photoanode are also presented in **a** and **b** (see figure legend). Conditions: **PSII** electrolyte solution, pH = 6.5, T = 25 °C. Counter and reference electrodes were a Pt wire and Ag/AgCl (3 M KCl), respectively.

Fig. 3 | Photocurrent action spectra of tandem PSII-dye photoanode. a, Single-wavelength action spectra of the IO-TiO$_2$|**dpp**|**P$_{Os}$**−**PSII** recorded with monochromatic light (λ_{scan}) measured in 20 nm steps from 760 nm to 420 nm (E_e = 6 mW cm^{-2}). The second left y-axis (grey) shows the corresponding external quantum efficiency (EQE) values. **b**, Dual-wavelength action spectra recorded with monochromatic light measured in 20 nm steps (E_e = 6 mW cm^{-2}) and a second simultaneous irradiation at a constant wavelength (λ_{const}) = 660 nm (E_e = 4 mW cm^{-2}). The action spectra were normalised to equal photon flux at 500 nm (0.26 mmol m^{-2} s^{-1}). The control experiments (with IO-TiO$_2$|**dpp**|**PSII**, IO-TiO$_2$|**dpp**|**P$_{Os}$** and IO-TiO$_2$|**P$_{Os}$**−**PSII** photoanodes) are also given. The right y-axis (blue) refers to the UV-Vis spectra of background-corrected **dpp** and **PSII** immobilised on the IO-TiO$_2$ electrodes (shaded in red and turquoise in the background). Conditions for all experiments: **PSII** electrolyte solution, pH = 6.5, T = 25 °C, E_{app} = 0.5 V vs. SHE. The error bars correspond to the standard deviation (N = 3).

Fig. 4 | Overall water splitting in semi-artificial PEC cell. a, Chronoamperometry (0.1 V voltage steps with 30 s dark and 30 s light cycles) of the two-electrode IO-TiO$_2$|**dpp**|**P$_{Os}$**−**PSII** ∥ IO-ITO|**H$_2$ase** cell. Applied voltage (U_{app}) values are shown on top of the lines. **b**, Photocurrent density as a function of U_{app} based on stepped-voltage (ΔU_{app} = 0.1 V) chronoamperometry measurements for IO-TiO$_2$|**dpp**|**P$_{Os}$**−**PSII** ∥ IO-ITO|**H$_2$ase** determined in **a**. Values of J were taken at the end of illumination (baseline-corrected for background dark current). Error bars correspond to the standard deviation (N = 3). **c**, Quantification of O$_2$ evolution (η_F = 88 ± 12%; N = 6) of the photoanode after continuous 1 h illumination (AM 1.5G filter; E_e = 100 mW cm^{-2}; λ > 420 nm) with continuous stirring at U_{app} = 0.3 V (red curve). The amount of H$_2$ (η_F = 82 ± 10%; N = 6) was quantified by GC analysis. Control experiments in absence of **PSII** (cyan trace) and without irradiation (black trace) are also shown. Conditions: **PSII** electrolyte solution, pH = 6.5, T = 25 °C, continuous stirring, N$_2$ atmosphere.

b

c

Photoanode
FTO|IO-TiO$_2$|dpp|P$_{Os}$–PSII

Cathode
FTO|IO-ITO|H$_2$ase

$h\nu_1$ 680 nm

$h\nu_2$ 496 nm

2 H$_2$O

O$_2$ + 4 H$^+$

Tyr$_Z$ Pheo$_{D1}$

Mn$_4$Ca

Q$_A$

P680

non-heme Fe

Q$_B$

Pheo$_{D2}$

C$_6$H$_{13}$

Et   Bu

Bu   Et

[4Fe4S]$_{dist}$

[4Fe4S]$_{med}$

[4Fe4S]$_{prox}$

NiFeSe

4 H$^+$ 2 H$_2$

Photosystem II (PSII)
$E_{O_2/H_2O} = +0.84$ V
$E_{Q_B/Q_B^-} = -0.06$ V

redox polymer (P$_{Os}$)
$E_{Os^{3+}/Os^{2+}} = +0.44$ V

dye (dpp)
$E_{dpp^*/dpp^-} = -1.17$ V
$E_{dpp^+/dpp} = +1.10$ V

IO-TiO$_2$
$E_{CB} = -0.55$ V
$E_g = 3.2$ eV

IO-ITO
$E_F = -0.55$ V

Hydrogenase (H$_2$ase)
$E_{H^+/H_2} = -0.39$ V

a

Light OFF (shaded), Light ON (white)

Potentials labeled: -0.5, -0.4, -0.3, -0.2, -0.1, 0.0, 0.1, 0.2, 0.3, 0.4, 0.5, 0.6, 0.7 V

y-axis: J / μA cm^{-2}
x-axis: time / s

b

y-axis: J / μA cm^{-2}
x-axis: E_{app} / V $vs.$ SHE

Legend:
- IO-TiO$_2$|**dpp**|**P$_{Os}$-PSII** (red ▶)
- IO-TiO$_2$|**dpp**|**PSII** (green ◆)
- IO-TiO$_2$|**dpp**|**P$_{Os}$** (blue ▼)
- IO-TiO$_2$|**P$_{Os}$-PSII** (black ◀)

a Single λ excitation λ_{scan} = 420-760 nm

b Dual λ excitation λ_{scan} = 420-760 nm
λ_{const} = 660 nm

IO-TiO$_2$|**dpp**|P$_{Os}$-PSII   IO-TiO$_2$|**dpp**|PSII

IO-TiO$_2$|**dpp**|P$_{Os}$ IO-TiO$_2$|P$_{Os}$-PSII

a

U_{app} →

Light OFF
Light ON

0.0   0.1   0.2   0.3   0.4   0.5 V

J / $\mu A\ cm^{-2}$

time / s

b

J / $\mu A\ cm^{-2}$

U_{app} / V

c

Light OFF
Light ON

$\eta_F(H_2) = 82 \pm 10\ \%$
$\eta_F(O_2) = 88 \pm 12\ \%$

n[O_2] / $\mu mol\ cm^{-2}$

time / min